

Rhombic Cell Analysis. II. Application to the IRAS/PSCz Catalogue

Tao Kiang¹, Yong-Feng Wu² and Xing-Fen Zhu²

¹ Dunsink Observatory, Dublin Institute for Advanced Studies, Dublin 15, Ireland;
tkiang@eircom.net

² Center for Astrophysics, University of Science and Technology of China, Hefei 230026

Received 2003 December 8; accepted 2004 January 30

Abstract Rhombic cell analysis as outlined in the first paper of the present series is applied to samples of varying depths and limiting luminosities of the IRAS/PSCz Catalogue. Numerical indices are introduced to summarize essential information. Because of the discrete nature of the analysis and of the space distribution of galaxies, the indices for a given sample must be regarded as each having an irreducible scatter. Despite the scatter, the mean indices show remarkable variations across the samples. The underlying factor for the variations is shown to be the limiting luminosity rather than the sampling depth. As samples of more and more luminous galaxies are considered over a range of some 2.5 magnitudes (a factor of some 75 in space density), the morphology of the filled and empty regions defined by the galaxies degrades steadily towards insignificance, and the degrading is faster for the filled than the empty region.

Key words: cosmology: large-scale structure of Universe — cosmology: observations — IRAS/PSCz catalogue

1 INTRODUCTION

This is the second paper in the series “Rhombic Cell Analysis”. Here we apply the technique described in Paper I (Kiang 2003) to the IRAS/PSCz Catalogue (Saunders et al. 2000, ‘PSCz’ hereinafter). The wealth of data in PSCz has meant that we can now apply the analysis to various depths (Sect. 2), and simultaneously to various limiting luminosities, since PSCz is flux-limited. The method developed so far centers on two number distributions, one of n_1 , the number of *like* neighboring cells to a given cell, and one of τ , a two-suffixed topological type, the two suffixes being the numbers of *like* and *unlike neighbor-groups*. Here in Sect. 3 we introduce four numerical indices, η on one hand, and χ_1 , χ_2 , χ_{21} on the other, intended to respectively summarise the most important characteristics of the two distributions. In Sect. 4 we shall point out an important circumstance in the practical application, namely, the n_1 - and τ - distributions depend rather sensitively on the precise location of the zero of the cells and that, as a consequence, each of the indices introduced above must be regarded as a random variable with a certain probability distribution. For each chosen sample of galaxies we consider a set of 16 independent zero offsets of the analysing cells and calculate the mean and standard

deviation of the four indices. And we do this separately for the sets of filled cells and empty cells. In Sect. 5 we plot the mean indices as functions of the sample depth, r_* . Remarkable features are found in the curves and their interpretation concludes this paper.

2 THE IRAS/PSCz CATALOGUE

The IRAS/PSCz Catalogue (Saunders et al. 2000) is the most comprehensive redshift catalogue to date. It covers 84% of the sky and contains about 15 000 galaxies to a uniform μ_{60} flux limit of 0.60 Jy. We counted 14 669 galaxies with measured (positive) redshifts z .

The 16% of the sky not covered by PSCz (the ‘‘gaps’’) consists of a large irregular zone of avoidance along the galactic equator, and two narrow stripes extending to high latitudes (Saunders et al., fig. 4). For our purpose the gaps must first be filled with mock galaxies. We are most grateful to Dr. Fabio Fontanot of Trieste for kindly providing us, before publication of the paper where it was used (Fontanot et al. 2003), with just such a list of 2808 mock galaxies, constructed according to a procedure given in (Branchini et al. 1999). The Fontanot list gives only the galactic coordinates and the redshifts; but we shall also be needing flux values. As we only need a random selection from the distribution of fluxes in PSCz, and as the Fontanot list is ordered quite independently of PSCz, we simply assigned every fifth value in PSCz to the Fontanot list. This ‘‘Filled-out PSCz catalogue’’ of $14669 + 2808 = 17477$ galaxies is the basic material for the present study.

We should point out that while a minor part of the data in the Fontanot list pertaining to the two narrow stripes were used in our work with the full weight (on an equal footing with the real PSCz data), the major part pertaining to the galactic zone of avoidance were used only in a diminished capacity (See Sect. 2.3). Similarly, the same diminished role is played by the small part of the PSCz data with $|b| < 10^\circ$.

2.1 Nominal Distance and Luminosity

We now have an all-sky catalogue of 17477 galaxies, each with a flux value and a redshift value. The next thing we do is to convert the redshifts into distances. For our purpose we can simply use a ‘‘nominal’’ distance, given by

$$r = cz/100 \quad (r \text{ in Mpc, } cz \text{ in km s}^{-1}). \quad (1)$$

This is because the subject-matter of our analysis, the number distributions of n_1 and of τ , ultimately depend only on the numbers of galaxies located inside a given (rhombic) cell and inside its twelve neighboring cells, so if we adopt a certain cosmology and use sophisticated formulae (of comoving distance for the cells, and of luminosity distance for the galaxies), the effect of so doing on the n_1 - and τ -distributions can be expected to be quite small, considering that PSCz only extends to $z \sim 0.1$.

With r so defined, we evaluate, for each galaxy, its usual rectangular coordinates $x = r \cos b \cos l$, $y = r \cos b \sin l$, $z = r \sin b$, and then, together with its flux f , its (nominal) luminosity L defined simply as $L = f \cdot r^2$ (other authors may prefer to add a factor of 4π here), or

$$\log L = \log f + 2 \log r, \quad (2)$$

where f is in Jy, and r is in Mpc.

2.2 Distance and Luminosity Limited Samples

In Paper I, the analysis was applied to the CfA catalogue, regarded as a single sample. At the end of that paper, the hope was expressed that with larger survey results becoming available, much finer analysis can be made. The PSCz has provided just such an opportunity.

PSCz is flux-limited. This means that within a distance-limited sample taken from PSCz, the coverage in luminosity is not uniform: it decreases with increasing distance. For uniformity, then, we should not take *all* the galaxies up to a certain distance r_* , but only those with luminosities greater than the corresponding limiting luminosity L_* , given by

$$\log L_* = \log 0.60 + 2 \log r_* . \quad (3)$$

Thus, each basic unit sample of our analysis satisfies *two* conditions, $r < r_*$ and $L > L_*$. In the $\log L \sim 2 \log r$ plane, such a sample is represented by a rectangular box with its lower right corner on the limiting diagonal. Such boxes generally overlap.

Our analysis is applied to eight such samples (Table 1). Each sample is identified by its limiting distance r_* , e.g., S-75, S-150, S-250 (Column 1). Their defining limiting luminosities are listed in Column 2. The eight samples cover a range of 0.52 dex in r_* , and a range of 1.04 dex (or 2.6 magnitudes) in L_* .

Table 1 Eight Distance- and Luminosity-Limited Samples

Sample (1)	$\log L_*$ (2)	a_0 (3)	$N_{fc}=N_{ec}$ (4)	$a_{0,\min}-a_{0,\max}$ (5)	ρ (10^{-6} Mpc^{-3}) (6)
S-75	3.53	7.173	780	7.072–7.296	1441.0
S-100	3.78	9.140	948	8.970–9.140	631.0
S-125	3.97	11.137	1020	11.034–11.204	301.0
S-150	4.13	13.856	925	13.730–14.220	150.0
S-175	4.26	16.762	797	16.393–16.762	84.9
S-200	4.38	19.750	737	19.340–19.982	49.3
S-225	4.48	22.970	660	22.898–23.340	29.4
S-250	4.57	27.620	492	27.070–27.620	18.3

2.3 An Illustrative Example

We take S-150 to illustrate the various steps in our calculation. First, to improve homogeneity of data, we define “actual used cells” by imposing, beside the condition $r < 150$, two further restrictions on the coordinates of the cell centres. 1) To avoid the large uncertainties in the inferred distances of the galaxies in our local “swimming pool”, we require $r > 25$. 2) To reduce undue influence of the mock galaxies in the galactic zone of avoidance, we require all the cells should be completely above latitude 10° . Now, our cells which can each be imagined as consisting of a cube of sides a_0 with its six faces covered by six pyramids of height $a_0/2$, are arranged along the galactic coordinate axes, so the second condition reads,

$$|z| > z_{\text{lim}} + a_0, \quad \text{where } z_{\text{lim}} = r \sin 10^\circ . \quad (4)$$

Thus, of the mock galaxies below 10° galactic latitudes, we made use of only those located in cells that share a common face with some cells completely inside the boundary, and then only in so far as they contribute to the definition of the like/unlike status of the common face. This remark applies also to those PSCz galaxies below latitude 10° .

With respect to the “outer” boundary of $r = 150$ in the present example of S-150, the need is obviously not so compelling that the actual used cells should be *completely* inside that boundary;—to require this would mean a substantial drop in the number of usable cells. So we define usable cells as those whose *centres* are within the $r = 150$ limit. Then our usable cells on the boundary will have parts outside that boundary, and moreover, the status of the “boundary” faces will further depend on the presence or absence of galaxies inside cells in the next shell out. It is easy to show that, for a given a_0 , if we consider all galaxies to a distance of $150 + (\sqrt{2} + 1)a_0$, then we will have included all relevant galaxies.

We find, by trial and error, the value of a_0 that will give equal numbers (or as equal as possible) of filled cells and empty cells, N_{fc} and N_{ec} of the actual usable cells. It is understandable that the two numbers are highly discontinuous functions of a_0 , and often a coarse adjustment succeeds where a fine-tuning fails. In the present case we found that $a_0 = 13.856$ succeeded in giving $N_{fc} = N_{ec} = 925$ (Table 1, Cols. 3, 4).

We can now summarise the various steps in this particular example of S-150. We start with the ‘filled-out PSCz catalogue’ of 17477 galaxies, and pick out those with $\log L \geq 4.13$ (Table 1, Line 4, Column 2). Then, for each trial value of a_0 , we determine the filled/empty status of all the cells with centres out to distance $150 + \sqrt{2}a_0$. Then, for the “actual used cells” with centres satisfying the three conditions, $25 \leq r, r \leq 150$, and the inequality (4), we count the number of filled cells, N_{fc} , and the number of empty cells, N_{ec} . We vary a_0 until N_{fc} and N_{ec} are equal (or as nearly equal as possible). Then for this optimal value of a_0 , we finally obtain the object of our analysis, the separate n_1 - and τ -distributions for the filled and empty cells.

The actual results in the present example are displayed in Figs.1 and 2. They can be compared with the figs.1 and 2 of Paper I. The final results of the present paper will be based on $8 \times 16 = 128$ such pairs of figures.

The values of the optimal a_0 for all the eight samples are given in Column 3 of Table 1. It happened that in all cases we had $N_{fc}=N_{ec}$. These equal values are listed in Column 4.

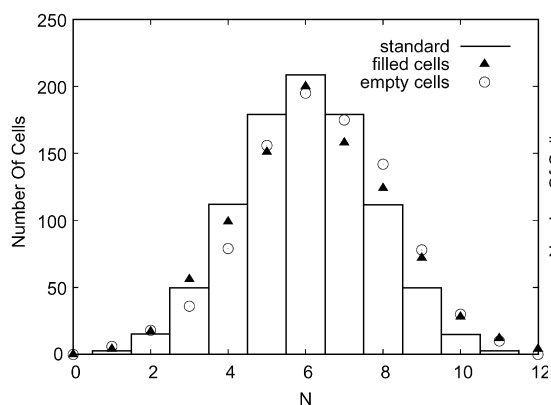


Fig. 1 The n_1 -distribution of the Illustrative Example. Histogram is the binomial distribution for the case of pure random mixture of filled and empty cells.

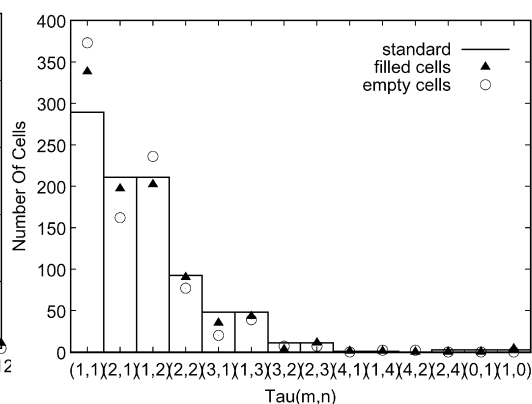


Fig. 2 The τ -distribution of the Illustrative Example. Histogram corresponds to the case of pure random mixture of filled and empty cells.

3 STATISTICAL INDICES

Our aim being comparison between the filled and empty regions of the universe based on their n_1 - and τ - distributions, it is obviously advantageous if we can summarise the most salient features of the distributions by some numerical indices. We have singled out one index, dubbed the “flocking index”, for the n_1 - distribution and three “ χ -type” indices for the τ -distribution.

3.1 The Flocking Index η

It was pointed out in Paper I (sect. 3.2.1) that, because of the imposed condition $N_{fc}=N_{ec}$, we must use some function of the observed n_1 frequencies other than the mean value $\langle n_1 \rangle$ as the “flocking index” η that quantifies the degree to which cells of the same kind (filled or empty) flock together.

Let us first rationalize the n_1 - distribution as follows: (i) We re-center the distribution at 0, i.e., we use a new independent variable, $k = n_1 - 6$, ($k = 0, \pm 1, \pm 2 \dots, \pm 6$). (ii) Because the frequency in the two end boxes ($k = \pm 6$) is usually very small, we put it into the next box, and regard the combined frequency as located at the “binomial” mean of the two, so now we have the rationalised distribution $N(k)$, defined for $k = 0, \pm 1, \pm 2, \pm 3, \pm 4, \pm 5, 228$.

Now, consider the five differences, $d_k \equiv N(|k|) - N(-|k|)$, $|k| = 1, 2, 3, 4, 5, 228$. Naturally, we would want our η to be positive when the d_k are generally more positive than negative; however, a straight sum of the five d_k would not be proper: they should each first be *standardized* by their expected random error. It seems reasonable, as a first approximation, to regard $N(|k|)$ and $N(-|k|)$ as two independent Poisson variables; then the variance of their difference would just be equal to their sum. Hence we standardize each difference by the square root of their sum, thus, $D(k) \equiv (N(|k|) - N(-|k|))/\sqrt{N(|k|) + N(-|k|)}$. But a straight sum of the $D(k)$ still does not seem quite right. Recalling the meaning of k , it seems reasonable that these standardized differences should each be given a weight equal to k . Thus, we finally arrive at our adopted formula for the flocking index η :

$$\eta = \sum kD(k) / \sum k, \quad k = 1, 2, 3, 4, 5, 228. \quad (5)$$

In words, η is a weighted average of standardized difference between the observed frequencies at equal and opposite distances from the centre of the n_1 - distribution, standardized with the expected random error of the difference, and weighted according to the distance from the centre. Note, the observed central frequency at $k = 0$ (or $n_1 = 6$) does not enter into the calculation of η .

3.2 The Three χ - type Indices

Our τ - distribution, being the number distribution of a two-parametered variable $\tau(m_1, m_2)$, does not lend itself to be similarly summarised by a single statistic. However, as was pointed out in Paper I, at the present stage of development of the rhombic cell analysis, we should perhaps concentrate on just 2 of the entries, namely, the two pertaining to $\tau(2, 1)$ and $\tau(1, 2)$, for these are respective signatures of one-ply strings and monolayers (Paper I, 3.2.2). Writing for short, the observed frequency of $\tau(2, 1)$ as $N(2, 1)$, and its expected frequency (expected on the assumption of a thorough mixture of filled and empty cells) as $E(2, 1)$, we define statistic

$$\chi_1 = (N(2, 1) - E(2, 1))/\sqrt{E(2, 1)}, \quad (6)$$

as a measure of the degree to which the observed frequency of one-ply string cells exceeds its random expectation.

Similarly, we define statistic

$$\chi_2 = (N(1,2) - E(1,2))/\sqrt{E(1,2)}, \quad (7)$$

in regard to the observed frequency of monolayer cells.

We have found it useful to introduce a third statistic that quantifies the difference $N(1,2) - N(2,1)$. Regarding the two as independent random variables, the proper standardized difference is

$$\chi_{21} = (N(1,2) - N(2,1))/\sqrt{N(1,2) + N(2,1)}, \quad (8)$$

which can be taken as a measure of the excess of “sheet cells” over “string cells”.

4 ZERO OFFSETS OF THE GRID OF CELLS

The present, more detailed application of rhombic cell analysis revealed a most important fact, which had no occasion of emerging in the preliminary application reported in Paper I. Namely, the n_1 - and τ - distributions are highly sensitive to the exact placing of the grid of rhombic cells, that is, to the zero offset. To explain, recall that our rhombic cells are defined in the following manner: space is first partitioned into a three-dimensional chessboard of black and white cubes of sides a_0 , all the white cubes are each cut into six pyramids, and a rhombic cell consists of a black cube with six white pyramids stuck on its faces. The centre of the rhombic cell coincides with the centre of the black cube. We label the cells by integer triplets (i, j, k) , with $i, j, k = 0, \pm 1, \pm 2, \dots$, subject to $i + j + k = 0 \pmod{2}$. We imagine the cells to form a rigid 3-d frame. We start our calculations by placing the centre of our zeroth cell $(0,0,0)$ at galactic coordinates $(0,0,0)$. What we found was that if we displace our entire grid of cells by an amount up to and including one unit of a_0 , in any combination of the three directions, then the resulting n_1 - and τ - distributions will generally be different, sometimes greatly so.

Now, the maximum displacement is one unit of a_0 either along one of the three axes, or along all three axes, (but NOT along two of the axes, which would reproduce the original grid). We denote this maximum displacement by $(1,1,1)$, and the original grid by $(0,0,0)$.

Let us now consider displacements involving half-units of a_0 , either positive or negative, in either 1, 2, or 3 of the 3 directions. There are altogether $3 \times 3 \times 3 - 1 = 26$ such displacements or offsets. But not all 26 are independent: some reproduce the same displacement of the grid. More precisely, the same displacement is obtained if we reverse the signs of any two non-zero displacements, e.g., the displacements or offsets $(+,0,-)$ and $(-,0,+)$ are duplicates of each other, and so are $(+,+,-)$ and $(-,+,+)$, and so on. In sum, 12 out of the 26 are duplicates, and 14 are independents.¹ Adding the original grid $(0,0,0)$ and the single one whole-unit displacement $(1,1,1)$, we have a total of 16 independent displacements or zero offsets.

Of course, so far we have been considering only displacements that involve half-units of a_0 . If, for example, we consider displacements involving quarter-units of a_0 , the number of independent displacements will then be much greater.

Each displacement or offset calls for a new evaluation of the optimal a_0 . We list, in Column (5) of Table 1, the largest and smallest a_0 among the 16 offsets for each of the considered samples. Each fresh value of a_0 results in fresh n_1 - and τ - distributions, and hence in fresh values of the indices $\eta, \chi_1, \chi_2, \chi_{21}$. Just to illustrate the effect of the offsets, we display in Table 2, the smallest and largest values of η and χ_{21} found among the 16 offsets, for the two

¹ The 14 independent offsets can be taken as $(0,0,+)$, $(0,0,-)$, $(0,+0)$, $(0,-0)$, $(+,0,0)$, $(-,0,0)$, $(0,+,+)$, $(0,+,-)$, $(+,0,+)$, $(+,0,-)$, $(+,+,0)$, $(+,-,0)$, $(+,+,+)$ and $(-,-,-)$.

samples S-100 and S-200, and for the filled and empty cells on separate lines marked “f” and “e”. We note that, in each case, the range is quite large.

Table 2 Smallest and Largest Values Among the 16 Independent Offsets

Sample	$\log L_*$	f/e	η		χ_{21}	
			min	max	min	max
S-100	3.78	f	2.12	3.63	3.14	7.40
		e	2.81	4.23	2.80	5.80
S-200	4.38	f	-1.17	0.54	-2.95	2.50
		e	-0.37	1.56	-0.92	2.60

4.1 Irreducible Scatter

On reflection, we should not be surprised by the fact that displacing the grid of cells slightly may result in drastically different n_1 - and τ - distributions. Consider, for example, two galaxies that are close together in space. Then, for one particular placement of the grid, the two may belong to one and same cell, while slightly shifting the grid may put them in two different cells; and the n_1 - and τ - distributions ultimately depend simply on how many galaxies go into which cells. We must now recognize the following fact of life: because of the ultimately discontinuous nature of the galaxy distribution in space, and because of the way the rhombic cell analysis works, a given sample of galaxies does not correspond to some one “true” value of an index, rather, it corresponds to a whole probability distribution of the index. In other words, each index has an irreducible scatter represented by some probability distribution, and the 16 values we get from the 16 independent offsets must be regarded as so many independent random samples taken from that parent distribution. And the most we can do is to estimate the mean and standard deviation (s.d.) of the parent distributions. Assuming normal distribution, the unbiased estimates of the mean and s.d. are given by the usual formulae²,

$$\langle x \rangle = \sum x_i/n, \quad \sigma = \sqrt{(\sum (x_i - \langle x \rangle)^2)/(n-1)}, \quad (n=16). \quad (9)$$

Here, x stands for any one of the four indices and the summation is over the 16 observed values x_i . We emphasize that, here, σ is an unbiased estimate of the s.d. of the hypothetical parent distribution; it is NOT the s.d. of the sample mean $\langle x \rangle$, usually known as “s.e.” (standard error). The latter would be equal to σ/\sqrt{n} , and so could be made very small by considering much larger values of n pertaining to displacements at smaller steps: its size thus largely depending on some man-made circumstance, it is inappropriate as an indicator of some objective scatter. On the other hand, the σ defined in (9), is an estimate of the irreducible scatter.

Our results, then, consist of the estimated mean and s.d. of the hypothetical distributions of the four indices, $\eta, \chi_1, \chi_2, \chi_{21}$, separately for the filled and empty cells of the eight selected distance/luminosity-limited samples. The results are listed in Table 3.

5 RESULTS INTERPRETATION

5.1 Formal Results

Remarkable trends emerge when the mean indices of Table 3 are plotted as functions of the sample depth r_* . See Figs. 3, 4, 5. In all the figures, filled triangles refer to filled cells, and open

² In a more strict notation, $\langle x \rangle$ would be written as $\hat{\mu}$, and σ , as $\hat{\sigma}$.

symbols, to empty cells. The error bars mark one unit of σ , the s.d. of the parent distribution defined at (9). In all cases, a trend is unmistakable despite the fact that each index for a given sample has quite a scatter as indicated by the size of the error bars.

Table 3 Results of Calculation for Selected Samples of PSCz Catalogue

Sample	$\log L_*$	f/e	η		χ_1		χ_2		χ_{21}	
			mean	s.d.	mean	s.d.	mean	s.d.	mean	s.d.
S-75	3.53	f	4.21	0.37	-4.49	0.91	3.00	0.78	5.46	1.02
		e	4.18	0.46	-4.11	0.80	0.95	0.85	3.80	0.78
S-100	3.78	f	2.83	0.40	-3.97	0.72	3.34	1.34	5.37	1.09
		e	3.51	0.41	-3.54	0.69	2.17	0.81	4.26	0.84
S-125	3.97	f	1.70	0.48	-2.62	1.34	1.83	0.70	2.75	0.96
		e	3.06	0.40	-2.58	1.11	2.18	1.22	3.38	1.46
S-150	4.13	f	1.39	0.54	-2.02	0.85	1.38	0.83	2.29	1.13
		e	1.79	0.48	-2.21	0.82	1.68	0.78	2.72	0.79
S-175	4.26	f	0.72	0.54	-0.68	1.15	0.32	0.83	0.72	1.07
		e	1.78	0.35	-2.01	0.73	1.16	0.92	2.24	0.96
S-200	4.38	f	-0.40	0.55	0.29	1.19	-0.17	1.03	-0.32	1.34
		e	0.77	0.53	-0.38	0.77	0.46	0.64	0.61	0.76
S-225	4.48	f	-0.73	0.51	0.22	0.58	-0.05	0.94	-0.51	0.66
		e	1.13	0.58	-0.64	0.93	0.92	1.02	1.39	0.80
S-250	4.57	f	-0.31	0.57	0.04	0.90	-0.08	0.91	-0.14	1.02
		e	1.08	0.55	-0.85	1.07	0.65	0.84	1.12	1.14

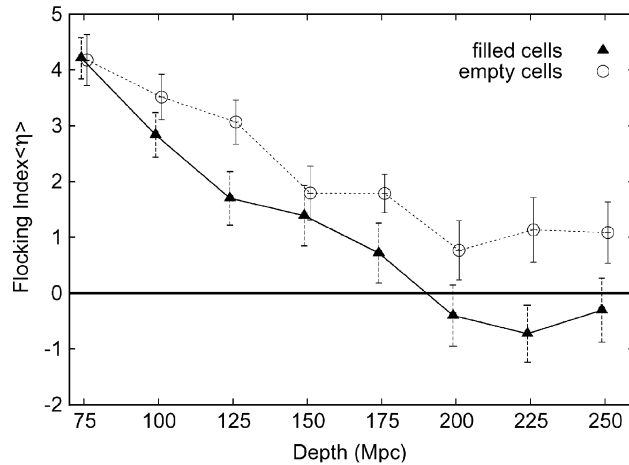


Fig. 3 Mean η as a function of the sample depth for filled and empty cells. Error bars mark 1 s.d. of the parent distributions.

5.1.1 The $\langle \eta \rangle \sim r_*$ Curve

Figure 3 shows the mean η versus sample depth curve, separately for the filled cells (filled triangles) and empty cells (open squares). There are two remarkable features. 1) Both curves start with definitely positive values at the smallest sample depth (75 Mpc), then both steadily fall with increasing depth. By 200 Mpc or so, the “filled curve” is marginally below the zero level of nil flocking, while the “empty curve”, marginally above. 2) While both curves fall steadily,

the empty curve remains consistently above the filled curve. Thus, for both the filled region and the empty region, there is a definite degree of likes flocking together at smaller depths, but the flocking decreases to insignificance around 200 Mpc. And, at any depth, the tendency of likes flocking together is stronger for the empty cells than for the filled cells.

Incidentally, for the single (inhomogeneous) CfA sample studied in Paper I, we have $\langle \eta \rangle = 2.09$ for the filled cells, and 4.02 for the empty cells. These can be seen to be entirely consistent with the curves of Fig. 1 at depths 75 ~ 100 and with the last statement.

5.1.2 The Three $\langle \chi \rangle \sim r_*$ Curves

Figures 4, 5, 6 show how each of the three χ -indices for the τ -distribution varies with the sample depth. First, Fig. 4 which refers to χ_2 , the degree to which the observed frequency of cells belonging to thin sheets (strictly, monolayers) exceed the random expectations (Eq. (7)).

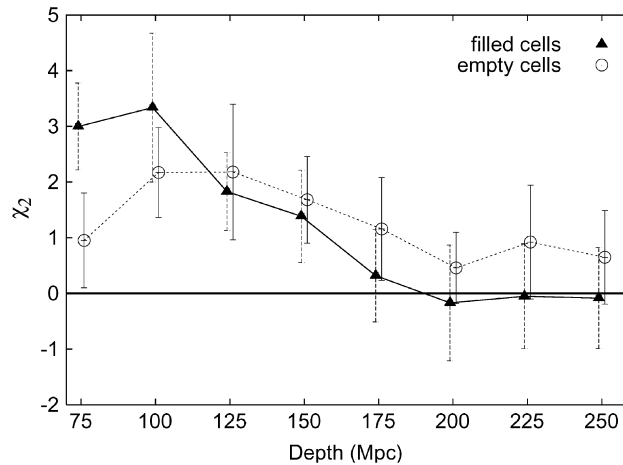


Fig. 4 Mean χ_2 as a function of the sample depth. Same symbols as in Fig. 3.

Figure 4 shows: at small depths, both the filled and empty curves are significantly positive, with the filled lying definitely above the empty. This last feature is consistent with a conclusion reached in Paper I, namely, the filled cells, but not the empty cells, show a tendency of occurring in sheets. In fact, we find, for the CfA data, $\langle \chi_2 \rangle = +2.38$ (filled), and -0.92 (empty). As the sample depth increases, both curves fall, the filled curve falling faster, so that at depths around 200 Mpc and beyond, the filled curve becomes entirely non-significant, while the empty curve remains marginally significant. The situation at large depths mimics the behaviour of the η -curves of Fig. 3; note, however, the larger error bars in Fig. 4.

Next, we consider the mean χ_1 versus depth curves shown in Fig. 5. Recall that χ_1 is a measure of the excess above random of the observed frequency of cells belonging to thin (one-ply) strings (Eq. (6)).

The χ_1 curves look like some mirror images of the χ_2 curves: they start significantly below the zero level and gradually rise to reach it around 200 Mpc, with the filled curve first below, then eventually above the empty curve. The values we found for the CfA data are $\langle \chi_1 \rangle = -3.81$ (filled) and -3.28 (empty), entirely consistent with the initial portions of the curves of Fig. 5.

The contrary behaviors of χ_2 and χ_1 suggested to us that an index for their difference may be of interest. Hence the index χ_{21} defined at (8). It could be called the “sheet-string

differential index”: it measures the excess of cells belonging to thin sheets over those belonging to thin strings, with no reference to their common random expectations.

The variation of mean χ_{21} with the sample depth is shown in Fig. 6. For the filled cells, we see that there is a considerable excess of “sheet cells” over “string cells” at small sample depths. As the sample depth increases, this excess becomes less and less, and eventually vanishes altogether at around 200 Mpc. For the empty cells, there is also a definite, though smaller, excess of “sheet cells” over “string cells” at the start, but the decrease with increasing depth is gentler in this case, such that even at the largest sample depths, there is still a small residual excess. Except for a short stretch at the beginning, the empty curve lies consistently above the filled curve, reminiscent of the $\langle \eta \rangle$ -curves of Fig. 3.

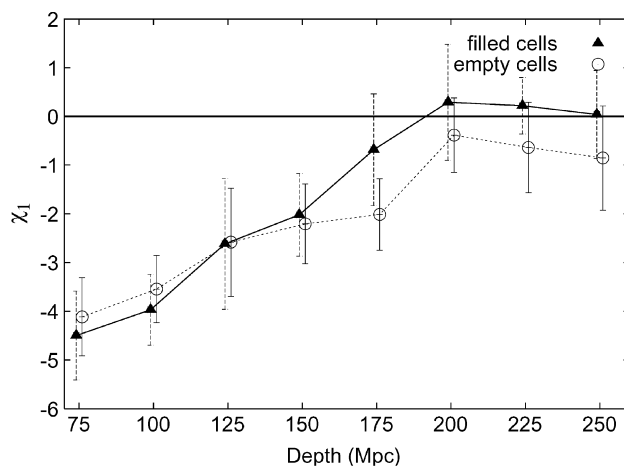


Fig. 5 Mean χ_1 as a function of the sample depth. Same symbols as in Fig. 3.

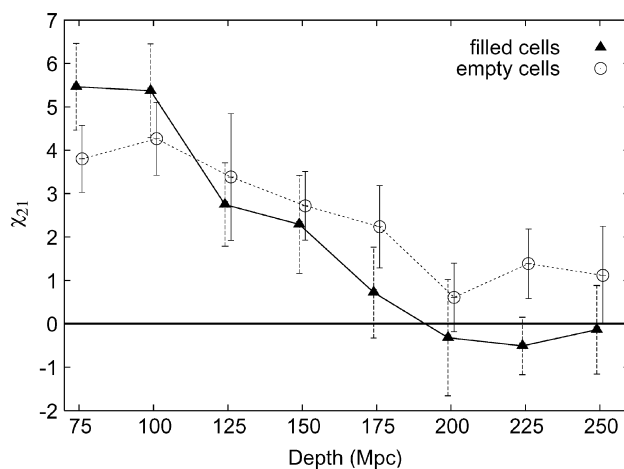


Fig. 6 Mean χ_{21} as a function of the sample depth. Same symbols as in Fig. 3.

5.2 Interpretation of Results

So far we have described the trends of the indices as variations with the sample depth, or the limiting distance of the sample. But this is for verbal convenience only. We have throughout this paper emphasized that each of our distance-limited samples is also a luminosity-limited sample, that as we consider deeper and deeper samples we are also considering samples of more and more luminous galaxies. Indeed, for the X-axis of our last four figures, we could equally have used the limiting luminosity instead of the limiting distance. So we must now address the question, “which of the two, limiting distance or limiting luminosity, is the parameter the morphology correlates with?”

This question is easily settled. All we have to do is to consider the *intersection* of two of our samples, and see how *its* results compare with those of the two original samples. We chose the intersection of S-100 and S-200. We call it S*-100, that is, the sample S*-100 has the same limiting distance as S-100 (100 Mpc) and the same limiting luminosity as S-200 ($\log L_* = 4.38$).

Table 4 compares the mean indices from S*-100 with those from S-100 and S-200 lifted from Table 3, separately for the filled regions (upper three lines) and the empty regions (lower three lines). It is clear that the results of S*-100 are much closer to those of S-200 than to those of S-100: the parameter that the morphology correlates with is *not* the sample depth; it is the limiting luminosity.

Table 4 Comparison of the Results of Three Samples

Sample	$\log L_*$	f/e	$\langle\eta\rangle$	$\langle\chi_1\rangle$	$\langle\chi_2\rangle$	$\langle\chi_{21}\rangle$
S-100	3.78	f	2.83	-3.97	3.34	5.37
S*-100	4.38	f	0.02	-0.33	0.16	0.35
S-200	4.38	f	-0.40	0.29	-0.17	-0.32
S-100	3.78	e	3.51	-3.54	2.17	4.26
S*-100	4.38	e	0.33	-0.44	0.85	0.83
S-200	4.38	e	0.77	-0.38	0.46	0.61

We must now re-state the empirical results obtained in the present study in the following terms. The morphology of the filled and empty regions defined by a given distance-and-luminosity-limited sample of galaxies is essentially a function of the limiting luminosity. As we consider samples of more and more luminous galaxies at ever decreasing space densities, the morphology degrades: the degree of like cells flocking together steadily decreases and so does the excess of cells belonging to thin sheets over those belonging to thin strings. And the degrading is generally stronger for the filled than for the empty region, so that one could say, at any luminosity level, the universe is always more like loose collections of lakes in a land than groups of islands and archipelagos in an ocean.

Recall that our luminosity is based on infrared flux and that its definition at (3) is purely nominal, it may be useful for future comparisons with results from other datasets to introduce a more objective parameter than the limiting luminosity L_* . We propose the space number density of galaxies more luminous than L_* , to be denoted by $\rho(L_*)$. This quantity is easily calculated: for it is simply the number of galaxies in the “filled-out PSCz Catalogue” (Sect. 2) with $r < r_*$ and $L > L_*$, divided by $(4/3)\pi r_*^3$. The results (in galaxies per $(100 \text{ Mpc})^3$) are given in the last column of Table 1.

5.3 A Density Effect or a Random Selection Effect?

It was suggested to us by the Referee that we should look into the possibility that the observed variation in the indices across the samples be a density effect (since, e.g., S-200 has

a smaller density than S-100) and that, for testing this possibility, we should use a random sample of S-100, labelled S** -100, with the same number of galaxies as S* -100.

As might be expected, the resulting indices varied much from one random selection to the next. So we took 10 such random selections. From now on, for simplicity, we shall restrict the discussion to one of the indices, and we choose the flocking index η for the filled region. We found, for the 10 random selections, η ranges from -0.85 to $+0.45$, with mean -0.24 and standard deviation 0.33 . Let us denote this mean value by η^{**} ; we have $\eta^{**} = -0.24$. This value is significantly smaller than the mean η for S-100 (which we now simply write as η_1 (from Table 3, $\eta_1 = 2.63$)).

Before interpreting this result ($\eta^{**} \ll \eta_1$), we should recall the reasoning behind our interpretation of a previous, formally similar inequality, we mean the inequality $\eta^* \ll \eta_1$, where η^* stands for the mean η for the sample S* -100 (according to Table 3, $\eta^* = 0.02$). And we interpreted this latter inequality as a luminosity effect because S* -100 simply consists of the more luminous members of S-100. Now, S** -100 is generated out of S-100 quite differently: we just pick out a certain prescribed number of its members, *purely at random*, without any regard to any individual properties. Hence, just as we interpreted the inequality $\eta^* \ll \eta_1$ as a luminosity effect, we must now interpret the inequality $\eta^{**} \ll \eta_1$ as an effect of random selection.

In fact, it seems quite plausible that any random selection of a population will be less “structured” than the population itself. Let us quantify the “degree of structuredness” by the ratio F_2/F_1 , with F_1 the fraction of isolated members and F_2 the fraction of members belonging to groups of 2 or more. Then it seems obvious that if we make a random selection of the population, with each member, whether isolated or belonging to a group, having the same chance of being selected, then the resulting F_2/F_1 will be smaller. This point that random selection destroys structure does not seem to have been noticed before in the literature; it provides a natural interpretation of our present finding, $\eta^{**} \ll \eta_1$.

Brief Summary The present study carries out one of the programs outlined at the end of Paper I, the application of rhombic cell analysis to a large size data. But more has been done. Statistical indices, particularly a “flocking index”, have been introduced to summarize much of the essential information and, after emphasising the discrete nature of the analysis and of the space distribution of galaxies, these indices for any given sample of galaxies are shown each to have an irreducible scatter. Despite the scatter, the indices showed remarkable variation with the limiting luminosity of the sample, leading to the conclusion stated above. It is planned to carry out further programs mentioned in Paper I, particularly the raising of the threshold of the filled cell.

Acknowledgements We thank the Referee for making a suggestion which led to a new insight as reported in Subsection 5.3. We thank Dr F. Fontanot of Trieste for making a list of mock galaxies available to us.

References

- Branchini E., Teodoro L., Frenk C. S. et al., 1999, MNRAS, 308, 1
- Fontanot F., Monaco P., Borgani S., 2003, MNRAS, 341, 692
- Kiang T., 2003, Chin. J. Astron. Astrophys., 3(2), 95
- Saunders W., Sutherland W. J. et al., 2000, MNRAS, 317, 55